J. Am. Soc. Mass Spectrom. (2018) 29:581–587
DOI: 10.1007/s13361-017-1874-x

RESEARCH ARTICLE

Matrix Assisted and/or Laser Desorption Ionization Quadrupole Ion Trap Time-of-Flight Mass Spectrometry of WO_3 Clusters Formation in Gas Phase. Nanodiamonds, Fullerene, and Graphene Oxide Matrices

Mayuri Vilas Ausekar,[1] Ravi Madhukar Mawale,[1] Pavel Pazdera,[1,2] Josef Havel[1]

[1]Department of Chemistry, Faculty of Science, Masaryk University, Kamenice 5/A14, 625 00, Brno, Czech Republic
[2]Center for Syntheses at Sustainable Conditions and Their Management, Faculty of Science, Department of Chemistry, Masaryk University, Kamenice 5/A14, 625 00, Brno, Czech Republic

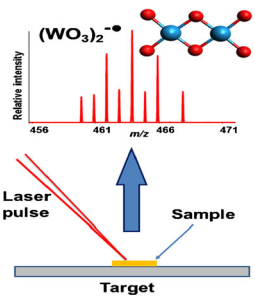

Abstract. The formation of $W_xO_y^{+\bullet/-\bullet}$ clusters in the gas phase was studied by laser desorption ionization (LDI) and matrix assisted laser desorption ionization (MALDI) of solid WO_3. LDI produced $(WO_3)_n^{+\bullet/-\bullet}$ (n = 1-7) clusters. In MALDI, when using nano-diamonds (NDs), graphene oxide (GO), or fullerene (C_{60}) matrices, higher mass clusters were generated. In addition to $(WO_3)_n^{-\bullet}$ clusters, oxygen-rich or -deficient species were found in both LDI and MALDI (with the total number of clusters exceeding one hundred ≈ 137). This is the first time that such matrices have been used for the generation of$(WO_3)_n^{+\bullet/-\bullet}$ clusters in the gas phase, while new high mass clusters $(WO_3)_n^{-\bullet}$ (n = 12-19) were also detected.

Keywords: WO_3 clusters, Laser desorption ionization, Quadrupole ion trap, TOF mass spectrometry, Fullerene C_{60}, Nano-diamonds, Graphene oxide matrices

Received: 12 May 2017/Revised: 15 December 2017/Accepted: 19 December 2017/Published Online: 16 January 2018

Introduction

Materials containing tungsten oxide are used in a wide range of applications because of their physical and chemical properties [1–8]. For example, the electrochromic properties of WO_3 underpins the development of WO_3/TiO_2 core-shell nanowires as an energy saving material in smart windows [4]. Graphene-WO_3 nanomaterials find uses in chemistry, including photo catalysis and NO_2 sensing, whereas the WO_3 building block forms the basis for polyoxometalate clusters with Keggin's and other structural forms, compounds which are highly prized for their redox and acid-base properties [8]. The possibility of discovering WO_3 based clusters with new structures and stoichiometry have driven a number of gas-phase studies using mass spectrometry-based methods. While LDI MS [9–12] and MALDI with classic matrices [13–15] have been used to generate tungsten oxide and molybdenum oxide clusters from various precursors, to the best of our knowledge, the formation of tungsten oxide clusters using carbonaceous matrices has not yet been reported. Here we have used LDI and MALDI with quadrupole ion trap time-of-flight mass spectrometry (QIT TOFMS) detection to study the formation of gas-phase tungsten oxide ($W_xO_y^{+\bullet/-\bullet}$) clusters from solid WO_3. The use of nonconventional carbonaceous matrices (nanodiamonds, fullerene, and graphene oxides) acting rather as SALDI or SELDI (surface assisted laser desorption ionization - or surface enhanced LDI) as a means of generating $W_xO_y^{+\bullet/-\bullet}$ clusters is also examined.

Experimental

Chemicals

Tungsten oxide powder (yellow color) was purchased from Lachema (Brno, Czech Republic). Acetonitrile, C_{60}, and nano-diamonds (NDs) were purchased from Sigma-Aldrich (Steinheim, Germany). Two different sources of graphene oxides (GOs) were used and these are designated as: (1) GO-1, which was purchased from Sigma-Aldrich (Steinheim,

Electronic supplementary material The online version of this article (https://doi.org/10.1007/s13361-017-1874-x) contains supplementary material, which is available to authorized users.

Correspondence to: Josef Havel; *e-mail:* havel@chemi.muni.cz

Germany); and (2) GO-2, which was donated by Grafenex Ltd. (Brno, Czech Republic). Red phosphorus was from Riedel de Haën (Hannover, Germany) and purified via sublimation in a vacuum [16]. Water (ultra-pure) was double distilled from a quartz apparatus of Heraeus Quarzschmelze (Hanau, Germany). All the other reagents were of analytical grade purity.

Mass Spectrometry

The mass spectra were recorded in both positive and negative ion modes by using an AXIMA Resonance mass spectrometer from Kratos Analytical Ltd. (Manchester, UK). This instrument was equipped with a quadrupole ion trap, which allows the recording of mass spectra in *m/z* ranges 100–400, 200–1200, 800–3500, 1500–8000, and 3000–15,000. It is equipped with a nitrogen laser (337 nm). The laser repetition rate was set to 5 Hz with a pulse width of 3 ns. The laser power was expressed in arbitrary unit (a.u.) from 0 to 180. The irradiated spot size was approximately 150 μm in diameter whereas the maximum laser power at 180 a.u. was 6 mW. Mass spectra were obtained by accumulating the spectra from at least 2000 shots. External calibration in the individual *m/z* ranges was done using red phosphorus clusters [16], whereas the accuracy achieved was ±10 mDa.

Software and Computation

Theoretical isotopic patterns were calculated using Launchpad software (Kompact ver. 2.9.3, 2011) from Kratos Analytical Ltd. (Manchester, UK). The structures of selective tungsten oxide clusters were visualized using Avogadro: an open source molecular builder and visualization tool [17].

Sample Preparation for MS Analysis

The target plate was cleaned several times with ethanol and then with double distilled water and dried at room temperature before sample deposition. For LDI measurement, 1 μL of WO_3 powder suspended in acetonitrile was deposited on the target plate and dried in a stream of air (Sample 1). Samples for MALDI were prepared by mixing WO_3 powder with copious amounts of ND, C_{60}, and graphene oxide matrices in an agate mortar and pestle and the resulting powders suspended in acetonitrile followed by 10 min of ultrasound and deposited in a similar way as for LDI (Samples 2, 3, and 4, respectively). The experimental setup of LDI and MALDI mass spectrometry for the generation of tungsten oxide clusters is shown in Figure 1.

The suspension of GO with WO_3 (Sample 4) was slightly greenish and settled on the bottom rather quickly (Supplementary Figure S1). Interestingly, when the WO_3 - GO mixture was heated (≈ 90–100 °C) under ultrasound, the formation of a stable dispersion was observed (even stable after several days). Sample 4 represents a kind of composite.

Results and Discussion

Mass spectra were recorded in both positive and negative ion modes. The effect of the laser energy for the LDI ionization of WO_3 and also for MALDI ionization with the use of carbonaceous matrices (MALDI) was studied for each *m/z* range and the laser energy at which the ionization starts was searched for. Spectra in negative ion mode are richer in WO_3 clusters than in the positive ion mode. With carbonaceous matrices, some carbon clusters were found. Results are given for the ranges *m/z* 100–400, 200–1200, 800–3500, and 1500–8000, while no significant signals were observed beyond *m/z* value 6000. The resolving power 5000–10 000 was achieved for all *m/z* ranges.

Range m/z 100–400

Positive Ion Mode

In positive ion mode, for all the samples (Samples 1–3) it was found that the ionization started at ~ 90–110 a.u. During laser ablation of Sample 1, $WO_2^{+\bullet}$ cation-radical was detected at around *m/z* 216 (value corresponds to the highest peak from the isotopic envelope). In the mass spectra of Sample 2**,** generation of $W^{+\bullet}$, $WO^{+\bullet}$, and $WO_2^{+\bullet}$ ions were observed (Supplementary Figure S2). In addition, a few low-intensity $WO_5H_3^-$ and $WO_5C^{-\bullet}$ ions were also detected. In the mass spectra obtained from Sample 3 no WO_3 clusters were observed, just a few carbon clusters were detected in agreement with the literature [18].

Negative Ion Mode

In negative ion mode, the ionization started at about 100–110 a.u. for all the samples. In the mass spectra recorded from the Sample 1 $WO_3^{-\bullet}$ ion was detected, while the most abundant peak detected was WO_4H^-. There was a good agreement between the experimental isotopic pattern and the theoretical model of mass spectra concerning $WO_3^{-\bullet}$ and WO_4H^- ions, which is shown in Supplementary Figure S3. $WO_5H_3^-$ and $WO_5C^{-\bullet}$ ions were also detected. In the mass spectra of Sample 2, in addition to the $WO_3^{-\bullet}$ ion, clusters of $WO_3H_8^-$, WO_4H^-, $WO_4H_{10}^-$, and $WO_5H_{10}^-$ were detected. When using C_{60} as matrix **(Sample 3),** only $(WO_3)_n^{-\bullet}$ (n = 1–3) clusters were detected. In addition, some peaks corresponding to clusters with higher numbers of oxygen, hydrogen, and carbon were detected. The appearance of hydrogen containing clusters $W_xO_yH_n$ is due to traces of water as moisture in the WO_3 preparative. Pavlov [10] observed a similar phenomenon and proposed a general formula $(WO_3)_nW_3(OH)_4(H_2O)_3(OH)^-$ for negatively charged clusters, abbreviated to $W_xO_yH_n^{+\bullet/-\bullet}$.

Range m/z 200–1200

Positive Ion Mode

In positive ion mode, the ionization for Samples 1-3 started at laser energy 120, 120, or 80 a.u., respectively. For the mass spectra of Sample 1, various series of clusters

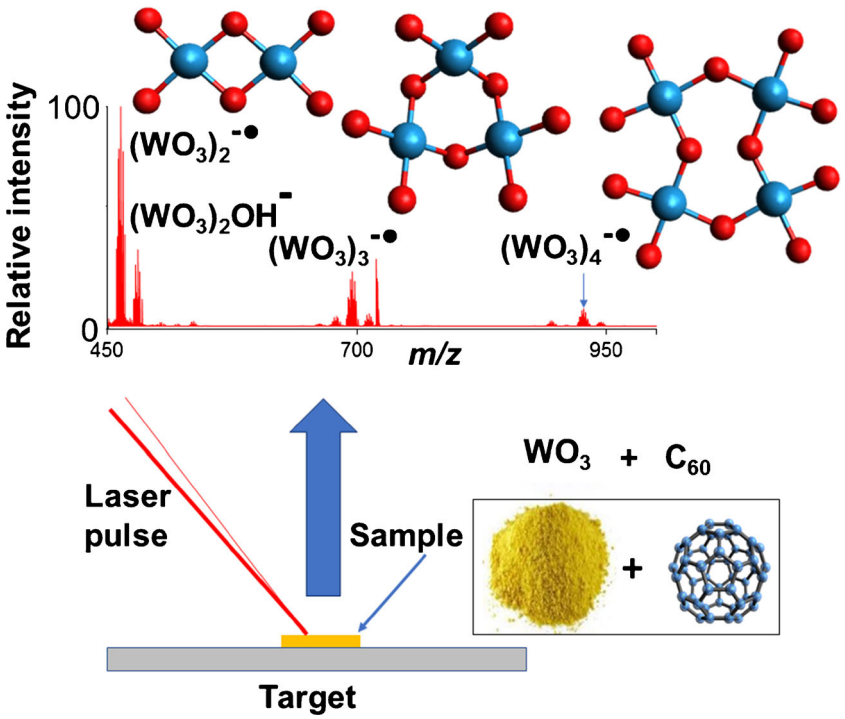

Figure 1. Experimental setup of LDI and/or MALDI TOF mass spectrometry for generation of tungsten oxide clusters. Structures of $(WO_3)_n$ were calculated using the Avogadro program [17]

$(WO_3)_n^{+\bullet}$ (n = 1–5); $(WO_3)_nW^{+\bullet}$ (n = 2–3); $(WO_3)_nWO^{+\bullet}$ (n = 2–3); $(WO_3)_nWO_2^{+\bullet}$ (n = 1–4) along with the species $(WO_3)_2W_2O_2^{+\bullet}$ and $(WO_3)_5H_2^{+\bullet}$ were detected (Supplementary Figure S4). The mass spectra obtained from Sample 2 were quite complex and difficult to interpret due to overlapping peaks and the partial appearance of hydrogen containing clusters. For Sample 3 some low intensive carbon clusters were detected.

Negative Ion Mode

In negative ion mode, the effect of laser energy was studied (Supplementary Figure S5) and the start of ionization was observed at 90–120 a.u. for all the samples. In the mass spectra of Sample 1, the series of polymeric $(WO_3)_n^{-\bullet}$ (n = 2–7) clusters was detected. Adjacent to each $(WO_3)_n^{-\bullet}$ peak, a series of clusters with the addition of one OH^- [$(WO_3)_nOH^-$ (n = 2–6)] was detected, in agreement with the literature [10], whereas a series of hydrogen and oxygen rich species were detected here for the first time (for example, $W_2O_8H_7^-$, $W_2O_9H_4^-$, $W_4O_{14}H_7^-$, and $W_4O_{15}H_9^-$). The peak intensities observed for the $W_3O_9^{-\bullet}$ cluster was congruent with those calculated (Supplementary Figure S6). Several "oxygen deficient species" with a lower number of oxygen atoms than in the $(WO_3)_n^{-\bullet}$ formula were detected, including $W_3O_6^{-\bullet}$, $W_3O_7^{-\bullet}$, and $W_3O_8^{-\bullet}$ clusters (e.g., inset in Figure 2a); and $W_4O_{10}^{-\bullet}$ and $W_4O_{11}^{-\bullet}$ clusters. From the mass spectra of Samples 2 and 3, series of clusters such as $(WO_3)_n^{-\bullet}$ (n = 1–5), were detected while several oxygen deficient series such as $W_2O_y^{-\bullet}$ (y = 5-8), $W_3O_y^{-\bullet}$ (y = 4-8), $W_4O_y^{-\bullet}$ (y = 7-11), and "hydroxylated" series [$(WO_3)_nOH^-$ (n = 2-5)] of clusters were also observed. Adjacent to each $(WO_3)_n^{-\bullet}$ species, related clusters arising from the addition of one OH^- and removal of one oxygen atom were observed (Figure 2a). In addition, clusters containing hydrogen/hydroxy group were also detected and these probably originate from traces of water present in the materials used. In the case of the MALDI experiments, the NDs or GO matrices may also be a source of both hydrogen and OH groups [19, 20].

Range m/z 800–3500

Positive Ion Mode

The ionization starts for all the samples at 80–100 a.u. In the mass spectra of Sample 1, a series of clusters: $(WO_3)_nWO_2^{+\bullet}$ (n = 3–6), $W_4O_{11}^{+\bullet}$, $W_4O_{12}H_2^{+\bullet}$, $W_5O_y^{+\bullet}$ (y = 13–14), $W_5O_{15}H_2^{+\bullet}$, $W_6O_y^{+\bullet}$ (y = 16–17), $W_6O_{20}H_{10}^{+\bullet}$, and $W_7O_y^{+\bullet}$ (y = 20–21) were detected. Figure 3 shows an overview of cluster peaks detected in the mass spectra obtained from Sample 1 in the range m/z 800–2000. The mass spectra obtained from Sample 2 are very complex due to overlapping of peaks, so even at the achieved mass resolution, the isotopic patterns of the clusters are not distinguishable. In the mass spectra obtained from Sample 3, there is an indication of the formation of carbon clusters with an even number of carbon atoms. Formation of carbon clusters shows that fullerene decomposition occurs.

Negative Ion Mode

In negative ion mode, the effect of laser energy has been studied, and the ionization starts for all three samples between 90 and 110 a.u. An example of the effect of laser energy for LDI of

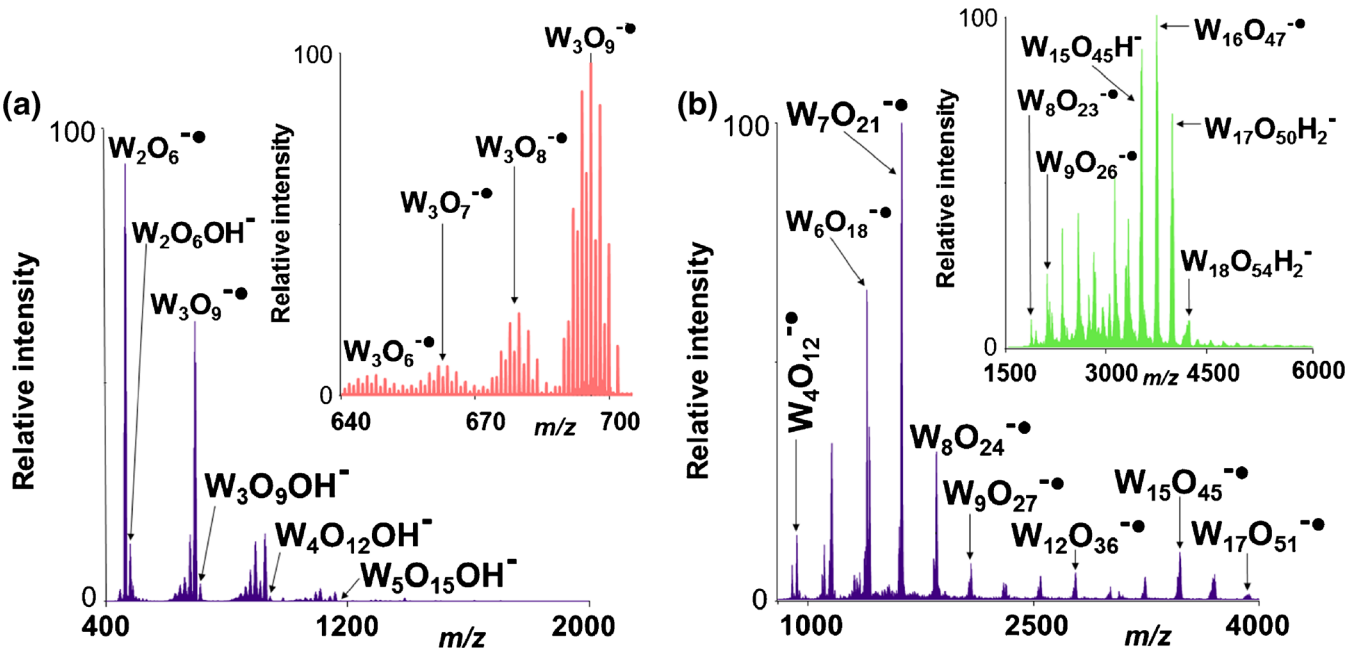

Figure 2. LDI mass spectrum of WO_3 when nano-diamonds were used as a matrix. **(a)** In the *m/z* range 400–2000 the series of clusters with increasing numbers of OH groups were identified. Another series with a lower number of oxygen is given in the inset. Conditions: negative ion mode, laser energy 140 a.u. **(b)** The *m/z* range 800–4000. Conditions: negative ion mode, laser energy 130 a.u. The mass spectrum in *m/z* range 1500–6000 is given in the inset. Conditions: negative ion mode, laser energy 150 a.u.

WO_3 (Sample 1) is given in Figure 4. For the mass spectra of Sample 1 series of clusters $(WO_3)_n^{-\bullet}$ ($n = 4$–8) was identified. In addition, several series of clusters deficient in oxygen and clusters containing hydrogen were also detected. Increasing the laser energy from 120 to 140, the intensity of the peaks in the range *m/z* 1500–2000 decreased, while the intensity of the peaks in the range *m/z* 800–1500 increased. A summary of $WxOyH_n^{+\bullet/-\bullet}$ clusters observed *via* LDI of WO_3 is given in Table 1 and overview of *m/z* values in Table 2.

From the mass spectra of Sample 2, a series of clusters $(WO_3)_n^{-\bullet}$ (n = 4–17) were identified (Figure 2b). In addition to this series, another one indicates clusters with a lower number of oxygen: $W_4O_y^{-\bullet}$ (y = 10–13), $W_5O_y^{-\bullet}$ (y = 13–14), $W_6O_y^{-\bullet}$ (y = 11–17), $W_7O_{20}^{-\bullet}$, $W_8O_{23}^{-\bullet}$, $W_9O_{26}^{-\bullet}$, $W_9O_{28}H^-$, and a series of clusters $W_5O_{15}OH^-$, $W_6O_{18}OH^-$, $W_7O_{21}OH^-$, and $W_8O_{24}OH^-$ containing hydroxyl were also detected. The mass spectra above *m/z* 2500 are complex and with low intensity. From the mass spectra of Sample 3 $(WO_3)_n^{-\bullet}$ (n = 4–8) clusters were detected

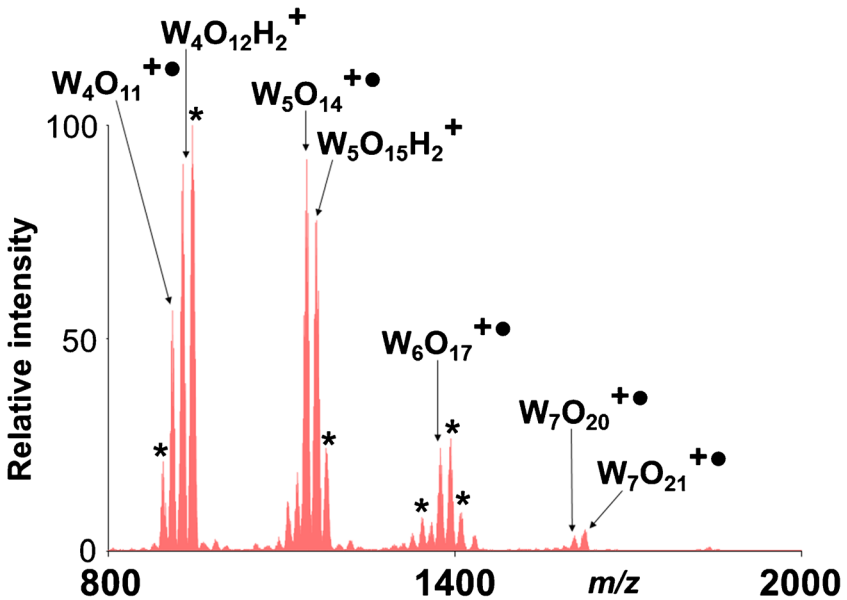

Figure 3. Overview of peaks detected in the mass spectra in mass range *m/z* 800–2000. Conditions: positive ion mode, laser energy 130 a.u. The peaks overlapped with hydrogen containing species are marked with an asterisk

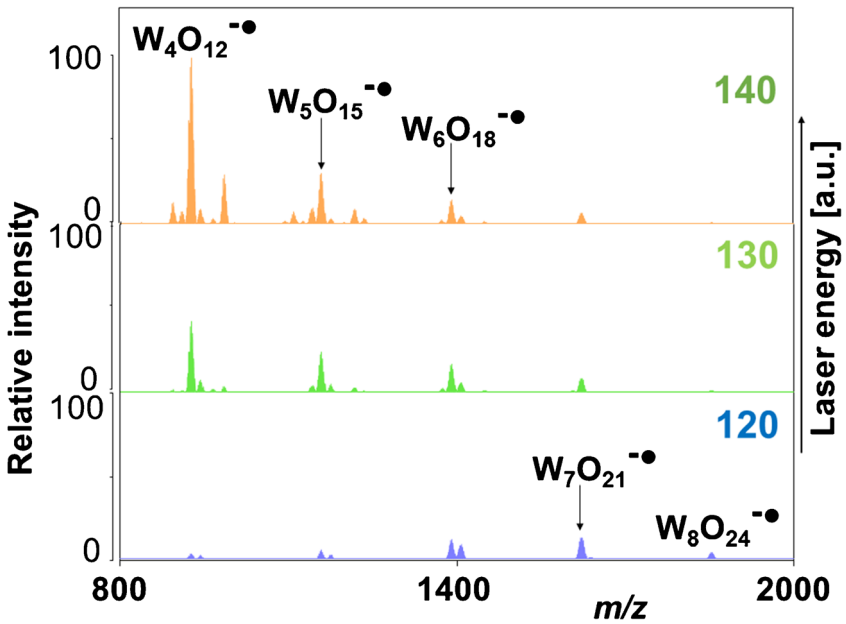

Figure 4. LDI mass spectra of WO_3 in the range *m/z* 800–2000. Effect of laser energy. Conditions: negative ion mode, spectra were normalized at 1500 mV, laser energy 120, 130, and 140 a.u.

(Supplementary Figure S7). In addition, some clusters with lower numbers of oxygen and hydroxyl group containing species were also detected similarly as described for Sample 2. From the comparison of LDI and MALDI mass spectra, it follows that from MALDI spectra (when using NDs as a matrix) clusters containing a higher number of tungsten oxide units were identified. Also, other $W_xO_y^{+\bullet/-\bullet}$ clusters are observed (Figure 5). This means that NDs as a matrix exhibit higher efficiency in the generation of $W_xO_y^{+\bullet/-\bullet}$ clusters compared with the fullerene C_{60} and/or LDI.

Range m/z 1500–8000

From the mass spectra of Sample 1 and Sample 3 – obtained in negative ion mode – no high *m/z* $W_xO_y^{-\bullet}$ clusters were identified while for Sample 2 $(WO_3)_n^{-\bullet}$ (n = 8–18) clusters were

Table 1. Overview of $(W_xO_y)H_n^{+\bullet/-\bullet}$ Clusters Detected from WO_3 during LDI and MALDI (NDs or Graphene Oxide Matrices)a

x	LDI	MALDI using NDs and GO as matrix
1	$WO_2^{+\bullet}$ $WO_5H_3^{+\bullet}$ $WO_3^{-\bullet}$ WO_4H^-	$W^{+\bullet}$ $WO^{+\bullet}$ $WO_2^{+\bullet}$ $WO_3^{-\bullet}$ WO_4H^+ $WO_5^{-\bullet}$ $WO_6^{-\bullet}$
2	$W_2O_5^{+\bullet}$ $W_2O_6^{+\bullet/-\bullet}$ $W_2O_7H^{+/-}$ $W_2O_9H_4^-$ $W_2O_{15}H^-$	$W_2O_6H^+$ $W_2O_7^{+\bullet}$ $W_2O_6^{-\bullet}$ $W_2O_7H^-$
3	$W_3O_6^{+\bullet}$ $W_3O_7^{+\bullet}$ $W_3O_8^{+\bullet/-\bullet}$ $W_3O_9^{-\bullet}$ $W_3O_9H_2^+$ $W_3O_{10}H_3^+$ $W_3O_{11}H_4^+$ $W_3O_{10}H^-$ $W_3O_{11}H_7^-$	$W_3O_{10}H_3^+$ $W_3O_9H_2^+$ $W_3O_{10}H^{+/-}$ $W_3O_4^{-\bullet}$ $W_3O_5^{-\bullet}$ $W_3O_6^{-\bullet}$ $W_3O_7^{-\bullet}$ $W_3O_8^{-\bullet}$ $W_3O_9^{-\bullet}$
4	$W_4O_8^{+\bullet}$ $W_4O_9^{+\bullet}$ $W_4O_{10}^{+\bullet/-\bullet}$ $W_4O_{11}^{+\bullet/-\bullet}$ $W_4O_{12}^{+\bullet/-\bullet}$ $W_4O_{13}H^{+/-}$	$W_4O_{10}^{+\bullet/-\bullet}$ $W_4O_{11}^{+\bullet/-\bullet}$ $W_4O_{12}H^+$ $W_4O_{13}H_3^+$ $W_4O_9^{-\bullet}$ $W_4O_{12}^{-\bullet}$ $W_4O_{13}H^-$
5	$W_5O_{11}^{+\bullet}$ $W_5O_{12}H_2^+$ $W_5O_{13}^{+\bullet}$ $W_5O_{14}^{+\bullet/-\bullet}$ $W_5O_{12}^{-\bullet}$ $W_5O_{13}^{-\bullet}$ $W_5O_{15}^{-\bullet}$ $W_5O_{15}H_2^+$ $W_5O_{16}H^-$	$W_5O_{14}^{-\bullet}$ $W_5O_{15}H^+$ $W_5O_{11}^{-\bullet}$ $W_5O_{12}^{-\bullet}$ $W_5O_{13}^{-\bullet}$ $W_5O_{14}^{-\bullet}$ $W_5O_{15}^{-\bullet}$ $W_5O_{16}H^-$
6	$W_6O_{15}^{+\bullet}$ $W_6O_{16}^{+\bullet/-\bullet}$ $W_6O_{17}^{+\bullet/-\bullet}$ $W_6O_{18}H_2^+$ $W_6O_{15}^{-\bullet}$ $W_6O_{18}^{-\bullet}$ $W_6O_{19}H^-$	$W_6O_{11}^{-\bullet}$ $W_6O_{12}^{-\bullet}$ $W_6O_{13}^{-\bullet}$ $W_6O_{14}^{-\bullet}$ $W_6O_{15}^{-\bullet}$ $W_6O_{16}^{-\bullet}$ $W_6O_{17}^{-\bullet}$ $W_6O_{18}^{-\bullet}$ $W_6O_{19}H^-$
7	$W_7O_{20}^{+\bullet/-\bullet}$ $W_7O_{21}^{+\bullet/-\bullet}$ $W_7O_{22}H^-$	$W_7O_{20}^{-\bullet}$ $W_7O_{21}^{+\bullet/-\bullet}$ $W_7O_{22}H^-$
8	$W_8O_{24}^{-\bullet}$ $W_8O_{23}^{-\bullet}$	$W_8O_{23}^{+\bullet/-\bullet}$ $W_8O_{24}^{-\bullet}$ $W_8O_{25}H^-$
9		$W_9O_{25}^{+\bullet}$ $W_9O_{26}^{-\bullet}$ $W_9O_{27}^{-\bullet}$ $W_9O_{28}H^-$
10		$W_{10}O_{29}^{-\bullet}$ $W_{10}O_{30}^{-\bullet}$
11		$W_{11}O_{32}^{-\bullet}$ $W_{11}O_{33}^{-\bullet}$
12		$W_{12}O_{36}^{-\bullet}$ **$W_{12}O_{41}^{-\bullet}$** **$W_{12}O_{42}^{-\bullet}$**
13		$W_{13}O_{39}^{-\bullet}$ **$W_{13}O_{44}^{-\bullet}$**
14		$W_{14}O_{42}^{-\bullet}$
15		$W_{15}O_{45}^{-\bullet}$
16		$W_{16}O_{48}^{-\bullet}$
17		$W_{17}O_{51}^{-\bullet}$
18		$W_{18}O_{54}^{-\bullet}$
19		**$W_{19}O_{57}^{-\bullet}$**

[a]Only major species with intensities three times higher than noise level are given here. The clusters in bold were detected only when graphene oxide was used as a matrix

Table 2. Overview of *m/z* Values for the most Intensive Clusters

Clusters	*m/z*	Clusters	*m/z*	Clusters	*m/z*
$WO_3^{+/-}$	232	$(WO_3)OH^{+/-}$	249	$(WO_3)\ H_2^{+/-}$	234
$(WO_3)_2^{+/-}$	464	$(WO_3)_2\ OH^{+/-}$	481	$(WO_3)\ H_2^{+/-}$	466
$(WO_3)_n$	$n \times 231.9$	$(WO_3)_n\ OH^{+/-}$	$231.9 \times n + 17$	$(WO_3)_n\ H_2^{+/-}$	$231.9 \times n + 2$

detected. There are also some low intensive clusters containing hydrogen, *e.g.*, $W_{15}O_{45}H^-$, $W_{17}O_{50}H_2^-$, $W_{18}O_{54}H_2^-$, etc. The detailed analysis of the mass spectra is given in inset of Figure 2b. The spectra above *m/z* ~4000 are of low intensity, complex, and difficult to resolve because of the overlapping of isotopic patterns of clusters. In the positive ion mode, no higher $W_xO_y^{+\bullet}$ clusters were detected.

MS Using Graphene Oxides as a Matrix

In addition to the use of nano-diamonds and C_{60} fullerene as matrices, the use of graphene oxides (GO-1 and GO-2) was also investigated by analyzing Sample 4. In negative ion mode, the 'richest' spectra with $(WO_3)_n^{-\bullet}$ (n = 1–19) clusters were obtained using GO-2 as a matrix (Supplementary Figures S8 and S9). In addition, oxygen rich and/or deficient species were detected similar to Sample 2. The spectra obtained in *m/z* range 1500–8000 using GO-1 as a matrix are complex. In positive ion mode, the spectra obtained from WO_3 using GO-1 were rich with various $W_xO_yH_n^{+\bullet/-\bullet}$clusters, while most of the species contained hydrogen. Using GO-1 and GO-2 as matrices, we also observed the formation $(W_{12}O_{41})^{-\bullet}$ and $(W_{12}O_{42})^{-\bullet}$ clusters. The caged-like dodecatungstate anion $(W_{12}O_{41})^{-\bullet}$ was described only when precursors such as $CaWO_4$, $PbWO_4$, WO_2, etc. were used in aqueous conditions, whereas with organic solvents such as acetonitrile or ethanol this caged $(W_{12}O_{41})^{-\bullet}$ cluster has not been detected [10, 12]. However, the highest mass clusters observed were the following: $W_9O_{27}^{-\bullet}$, $W_{10}O_{30}^{-\bullet}$, $W_{11}O_{33}^{-\bullet}$, $W_{12}O_{36}^{-\bullet}$, $W_{12}O_{41}^{-\bullet}$, $W_{12}O_{42}^{-\bullet}$, $W_{13}O_{44}^{-\bullet}$, $W_{14}O_{42}^{-\bullet}$, $W_{15}O_{45}^{-\bullet}$, $W_{16}O_{48}^{-\bullet}$, $W_{17}O_{51}^{-\bullet}$, $W_{18}O_{54}^{-\bullet}$, and $W_{19}O_{57}^{-\bullet}$.

Remark: "The differences in the types of ions observed using different matrices can be ascribed to the fact that nanodiamonds, fullerene, and GO1 or GO2 do not work the same way as classic MALDI matrices but rather as SALDI or SELDI (surface assisted or surface enhanced) materials, which increase the efficacy of laser desorption ionization [21, 22]."

MS^n Analysis

The analysis of selected ions in the gas phase was also done by MS^2. For example, collision-induced dissociation (CID) of the cluster at around *m/z* 927.8 $(WO_3)_4^{-\bullet}$ leads to the formation of product ions at around *m/z* 463.9 $(WO_3)_2^{-\bullet}$ corresponding to the loss of $(WO_3)_2$ at around (463.9 Da) as demonstrated in Supplementary Figure S10.

The Structure of $(W_xO_y)H_n^{+/-}$ Clusters

TOF MS does not give direct structural information on the clusters. Some structures of $(W_xO_y)H_n^{+\bullet/-\bullet}$ clusters have already been described [1, 23–25], and some of these are shown in Figure 1. Although the high mass clusters found here may be

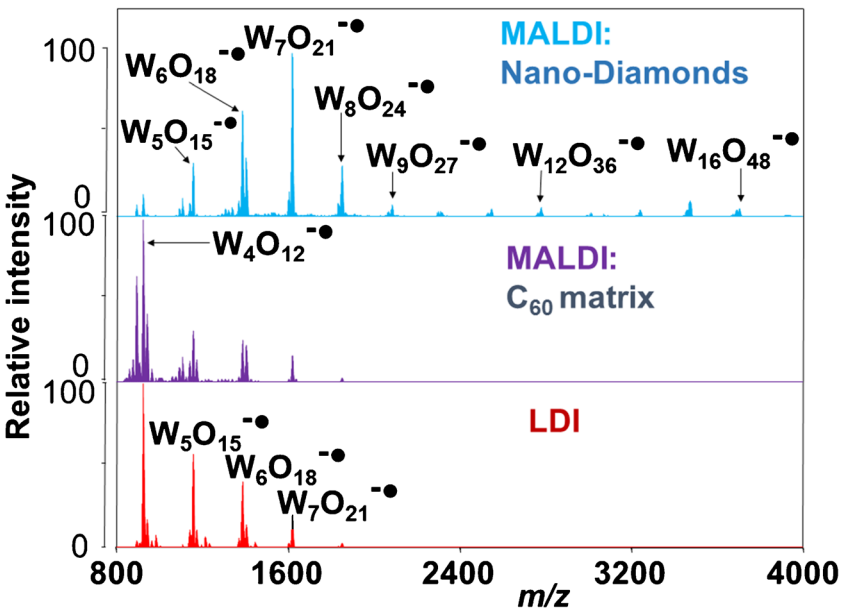

Figure 5. Comparison of LDI and MALDI mass spectra of WO_3 when using either C_{60} or NDs matrices in the *m/z* range 800–4000. Conditions: negative ion mode, laser energy 130 a.u.

structurally related to $W_2O_8^-$ and $W_3O_n^-$ (n = 7–11) previously studied using computational chemistry, a detailed quantum chemistry study would provide valuable information on how the structure of these clusters vary based upon the number of oxygen atoms present. Such a study is beyond the scope of this work.

Conclusions

LDI with QIT TOF MS detection was found to be a powerful technique for the generation and analysis of $(WO_3)_n$ clusters. NDs or graphene oxide as MALDI matrices exhibit the highest efficiency for the generation of high mass WO_3 clusters compared with fullerene and direct LDI of WO_3 and, for the first two matrices, the formation of $(WO_3)_n^{-\bullet}$ (n = 1-19) clusters was demonstrated. The increase of ionization can be explained by the SALDI or SELDI effect. The highest increase is observed in nano-diamonds and graphene oxide. Anionic $(WO_3)_n^{-\bullet}$ (n = 12-19) clusters and some cationic clusters such as $(WO_3)_n^{+\bullet}$ (n = 1-7) are reported here for the first time. The formation of caged-like dodecatungstate anions was observed when using GO as a matrix. Knowledge concerning the formation of tungsten oxide clusters in the gas phase might be important for the development of various new materials.

Acknowledgments

The authors thank Grafenex Ltd. (Brno, Czech Republic; e-mail: mirek.pitrocha@grafenex.cz) for providing samples of graphene oxides. M.A. thanks the South Moravian Center (JCMM) for providing a scholarship. Dr. L. Prokeš is thanked for his help with mass spectra measurements.

References

1. Zheng, H., Ou, J.Z., Strano, M.S., Kaner, R.B., Mitchell, A., Kalantar-Zadeh, K.: Nanostructured tungsten oxide - properties, synthesis, and applications. Adv. Funct. Mater. **21**, 2175–2196 (2011)
2. Buch, V.R., Chawla, A.K., Rawal, S.K.: Review on electrochromic property for WO_3 thin films using different deposition techniques. Mater. Today Proc. **3**, 1429–1437 (2016)
3. Gavrilyuk, A.I.: Aging of the nanosized photochromic WO_3 films and the role of adsorbed water in the photochromism. Appl. Surf. Sci. **364**, 498–504 (2016)
4. Huang, B.R., Lin, T.C., Liu, Y.M.: WO_3/TiO_2 core-shell nanostructure for high performance energy-saving smart windows. Sol. Energy Mater. Sol. Cells. **133**, 32–38 (2015)
5. Zhou, M.-J., Zhang, N., Hou, Z.H.: A facile synthesis of graphene-WO_3 nanowire clusters with high photocatalytic activity for O_2 evolution. Int. J. Photoenergy. **2014**, 1–6 (2014)
6. He, G.H., He, G.L., Li, A.J., Li, X., Wang, X.J., Fang, Y.P., Xu, Y.H.: Synthesis and visible light photocatalytic behavior of WO_3 (core)/Bi_2WO_6 (shell). J. Mol. Catal. A Chem. **385**, 106–111 (2014)
7. Xiaoqiang, A., Jimmy, C.Y., Wang, Y., Yongming, H., Xuelian, Y., Zhang, G.: WO_3 nanorods/graphene nanocomposites for high-efficiency visible-light-driven photocatalysis and NO_2 gas sensing. J. Mater. Chem. **22**, 8525–8531 (2012)
8. Pope, T.M.: Happy Birthday Keggin Structure. Eur. J. Inorg. Chem. **2013** (10–11), (1561)
9. Singh, D.M.D.J., Pradeep, T., Thirumoorthy, K., Balasubramanian, K.: Closed-cage tungsten oxide clusters in the gas phase. J. Phys. Chem. A. **114**, 5445–5452 (2010)
10. Pavlov, J., Braida, W., Ogundipe, A., O'Connor, G., Attygalle, A.B.: Generation and detection of gaseous $W_{12}O_{41}^{-\bullet}$ and other tungstate anions by laser desorption ionization mass spectrometry. J. Am. Soc. Mass Spectrom. **20**, 1782–1789 (2009)
11. Pavlov, J., Attygalle, A.B.: Laser ionization mass spectrometry of inorganic ions. In: Mike, S.L. (ed.) Mass Spectrometry Handbook, pp. 1207–1227. John willey & Sons Inc., Hoboken (2012)
12. Lunk, H.J.: Comment on: "Generation and Detection of Gaseous $W_{12}O_{41}^{-\bullet}$ and other Tungstate Anions by Laser Desorption Ionization Mass Spectrometry". J. Am. Soc. Mass Spectrom. **21**, 1466–1467 (2010)
13. Bai, Y.P., Liu, S., Song, F.R.: Formation of tungstate-containing cluster ions by polyoxotungstate anions under matrix-assisted laser desorption/ionization condition in the gas phase. Rapid Commun. Mass Spectrom. **25**, 3504–3508 (2011)
14. Bai, Y.P., Liu, S., Song, F.R.: Generation of tungstate ion clusters by Keggin-type silicopolyoxotungstate anions under matrix-assisted laser desorption/ionization condition in the gas phase. Rapid. Commun. Mass Spectrom. **26**, 715–718 (2012)
15. Xu, R.-F., Bai, Y.-P., Lian, W.-H., Liu, S., Song, F.-R., Liu, Z.-Q., Liu, S.-Y.: Tungstate-containing clusters ions in the gas phase by MALDI-FTICRMS. Chem. J. Chin. Univ. **34**, 1106–1110 (2013)
16. Sládková, K., Houška, J., Havel, J.: Laser desorption ionization of red phosphorus clusters and their use for mass calibration in time-of-flight mass spectrometry. Rapid Commun. Mass Spectrom. **23**, 3114–3118 (2009)
17. Hanwell, M.D., Lonie, D.C., Vandermeersch, T., Zurek, E., Hutchison, G.: Avogadro: an advanced semantic chemical editor, visualisation, and analysis platform. J. Chem. Informatics. **4**(17), 1–**17** (2012)
18. Šedo, O., Alberti, M., Janča, J., Havel, J.: Laser desorption-ionization time of flight mass spectrometry of various carbon materials. Carbon. **44**, 840–847 (2006)
19. Mochalin, V.N., Shenderova, O., Ho, D., Gogotsi, Y.: The properties and applications of nanodiamonds. Nat. Nanotechnol. **7**, 11–23 (2012)
20. Dreyer, D.R., Park, S., Bielawski, C.W., Ruoff, R.S.: The chemistry of graphene oxide. Chem. Soc. Rev. **39**, 228–240 (2010)
21. Wang, J., Liu, Q., Liang, Y., Jiang, G.: Recent progress in application of carbon nanomaterials in laser desorption/ionization mass spectrometry. Anal. Bioanal. Chem. **408**, 2861–2873 (2016)
22. Tang, L.A.L., Wang, J., Loh, P.K.: Graphene-based SELDI robe with ultrahigh extraction and sensitivity for DNA Oligomer. J. Am. Chem. Soc. **132**, 10976–10977 (2010)
23. Huang, X., Zhai, H.-J., Li, J., Wang, L.-S.: On the structure and chemical bonding of tri-tungsten oxide clusters $W_3O_n^-$ and W_3O_n (n = 7-10): W_3O_8 as a potential molecular model for O-deficient defect sites in tungsten oxides. J. Phys. Chem. A. **110**, 85–92 (2006)
24. Lin, S.J., Cheng, J., Zhang, C.F., Wang, B., Zhang, Y.F., Huang, X.: The reactivity of stoichiometric tungsten oxide clusters towards carbon monoxide: the effects of cluster sizes and charge states. Phys. Chem., Chem. Phys. **17**, 11499–11508 (2015)
25. Huang, X., Zhai, H.-J., Waters, T., Li, J., Wang, L.-S.: Experimental and theoretical characterization of superoxide complexes $[W_2O_6(O_2^-)]$ and $[W_3O_9(O_2^-)]$: models for the interaction of O_2 with reduced W sites on tungsten oxide surfaces. Angew. Chem. Int. Ed. Engl. **45**, 657–660 (2006)